J Opt
https://doi.org/10.1007/s12596-023-01565-4

RESEARCH ARTICLE

Enhanced laser wakefield acceleration utilizing Hermite–Gaussian laser pulses in homogeneous plasma

Vivek Sharma[1] · **Vishal Thakur**[1]

Received: 16 September 2023 / Accepted: 26 November 2023

Abstract The paper investigates the phenomenon of laser wakefield acceleration in a collisionless underdense plasma using Hermite–Gaussian laser pulses. Laser wakefield acceleration is a promising method to generate high-energy particle beams over short distances. The study focuses on utilizing Hermite–Gaussian laser pulses, which have a unique intensity distribution, to drive the wakefield and accelerate electrons effectively. Through theoretical analysis, the paper explores the intricate interplay between the laser pulse's characteristics, the resulting laser wakefield structure, and the electron energy gain. In our research, we revealed that the electron energy gain rises as the amplitude of the laser pulse increases irrespective of Hermite mode index (s). Under identical conditions, we observed enhanced energy gain for s = 0 and s = 2 mode indexes than for s = 1 mode. Electron energy gain varies with pulse length, plasma density, and beam waist for a given Hermite mode index. As a result, the optimized value of any one parameter for maximum energy gain fluctuates with the corresponding values of the other two parameters as well. We have successfully obtained an energy gain of 2.65 GeV with a selected set of parameters. The findings shed light on the potential of Hermite–Gaussian laser pulses in enhancing the performance of laser wakefield acceleration setups, offering insights into optimizing the generation of high-energy particle beams for various applications, such as particle physics experiments and medical treatments.

Keywords Laser wakefield acceleration · Laser pulse shape · Gaussian-like laser pulse · Energy gain · Energy efficiency

Introduction

In the modern era, accelerated charged particles can be considered as back bone of scientific research and development. In the realm of materials science, accelerated electrons enable high-resolution imaging and characterization [1], facilitating breakthroughs in nanotechnology [2], catalysis, and material design [3]. In medical science, their application in radiation therapy has revolutionized cancer treatment, allowing for precise tumor targeting while minimizing damage to surrounding healthy tissues [4]. Furthermore, accelerated electrons play a pivotal role in particle physics research, aiding in the exploration of fundamental particles and their interactions, thus expanding our understanding of the universe's building blocks[5].The energy sector benefits from accelerated electrons through enhanced insights into materials for energy storage, conversion, and generation, fostering advancements in renewable energy technologies[6]. In environmental science, their utilization contributes to the development of novel pollution control methods and pollutant degradation processes [7]. Accelerated electrons also find their place in the preservation and restoration of cultural heritage artifacts, offering noninvasive analysis and cleaning techniques [8].

Due to such important applications, several energy efficient particle acceleration techniques have been developed and continuous efforts have been made to further improve these techniques. Tajima et al. [9] had proposed the mechanism to generate plasma waves with the help of intense laser pulse in underdense plasma. Tera hertz generation

✉ Vishal Thakur
vishal20india@yahoo.co.in

[1] Department of Physics, Lovely Professional University, G.T. Road, Phagwara, Punjab 144411, India

Published online: 30 December 2023

[10]–[16], second harmonic generation [17, 18], third harmonic generation[19, 20], self-focusing[21, 22] and electron acceleration[23, 24] are some of achievable phenomenon of plasma waves generated by laser–plasma interaction.

Recently, the use of electric field, magnetic field, and carbon nano-tubes has made a revolutionary change in nonlinear interaction phenomenon shown by laser–plasma interaction [15]–[13]. Under controlled conditions, this plasma wave can be utilized to accelerate electrons also. Laser pulse can carry energy with extremely high intensity in a controlled manner and plasma is an ultimate source of free electrons to be accelerated. Plasma provides a medium also, in which the collective behavior of charges can be utilized to accelerate electrons to a very high relativistic energy level.

Direct laser action (DLA), beat wave acceleration in vacuum and plasma (BWA), plasma wake field accelerator (PWFA) and laser wakefield acceleration (LWFA) are dominant acceleration techniques to obtain electrons of relativistic energy[25]. Fallah et al. [26] have used Bessel–Gaussian pulse to investigate electron acceleration and found that Bessel–Gaussian pulse produces effective electron acceleration. Sharma et al.[27, 28] have studied the effect of frequency chirp on LWFA and found that phenomenon of LWFA can be enhanced using positive chirp. Varaki et al. [29] have compared electron acceleration produced by Gaussian, Super-Gaussian, and Bessel–Gaussian pulse in the presence of wiggler magnetic field. Sharma et al.[33] have observed the enhancement in LWFA when oblique magnetic field is applied with a circular polarized pulse. Ghotra [31] has studied the combined effect of LWFA and direct laser acceleration on electron acceleration phenomenon.

Use of static or wiggler magnetic field, positive/negative or linear/quadratic frequency chirp, slanting or ripped plasma density, laser pulse profile, laser pulse length, laser strength are some of the important parameters which have direct impact on acceleration process[32]–[36].

In the present study, we have used Hermite–Gaussian laser pulse propagating through cold, collisionless, underdense homogeneous plasma. Homogeneous plasma refers to plasma with uniform density and composition. Such plasma improves acceleration consistency, reduces energy spread and minimizes plasma instabilities. It is easier to generate homogeneous plasma experimentally. These are some of the benefits of choosing homogeneous plasma as a medium for LWFA. Using equation of motion, continuity equation and Maxwell's equation, solutions for wake potential, wakefield and energy gained by electrons are derived analytically. The effect of pulse length, laser intensity, plasma density, and Hermite–Gaussian mode index on LWFA is studied Curves are plotted to discuss and compare the results. Analytical solution is given in section II. Curves are plotted and outcomes are discussed in result and conclusion section III. Conclusions are given section IV of the paper. The paper ends with the references.

Analytical solution of LWFA

We explore the propagation of a laser pulse of an electric field (E) and a magnetic field (B) along the z-axis in homogeneous underdense collisionless plasma. The following fundamental equation of motion is used to create laser–plasma interaction.

$$\Rightarrow \frac{\partial \vec{P}}{\partial t} + \left(\vec{V}.\vec{\nabla}\right)\vec{P} = -e\left\{\vec{E} + \vec{V} \times \vec{B}\right\} \tag{1}$$

Here, e is electric charge, $\vec{V}$ is velocity of electron, $\vec{P} = \gamma m_0 \vec{V}$ is relativistic momentum of electrons, m_0 is rest mass of electron, relativistic factor γ is given by

$$\gamma = \frac{1}{\sqrt{1 - \frac{V^2}{C^2}}} = \sqrt{1 + \left(\frac{P}{mc}\right)^2} \tag{2}$$

Here, c is speed of light. $V_\parallel$ and $V_\perp$ are velocity components along (z-direction) and perpendicular (x-direction) to the laser propagation direction then,

$$\vec{V} = V_\perp \hat{i} + V_\parallel \hat{k} \tag{3}$$

$$\text{z} - \text{ component of momentum } P_\perp = \frac{m_0 V_\perp}{\sqrt{1 - \frac{\left(V_\parallel^2 + V_\perp^2\right)}{c^2}}} = \frac{m_0 V_\perp}{\sqrt{1 - \frac{V_\perp^2}{c^2}}} \approx m_0 V_\perp \tag{4}$$

$$\text{x} - \text{ component of momentum } P_\parallel = \frac{m_0 V_\parallel}{\sqrt{1 - \frac{\left(V_\parallel^2 + V_\perp^2\right)}{c^2}}} = \frac{m_0 V_\parallel}{\sqrt{1 - \frac{V_\perp^2}{c^2}}} \approx m_0 V_\parallel \tag{5}$$

Solving Eq. (1) using (3) to (5), we get

$$\frac{\mathrm{d}V_\parallel}{\mathrm{dt}} + V_\parallel \frac{\partial V_\parallel}{\partial z} = \frac{e}{m_0}\frac{\partial \Phi}{\partial z} - \frac{eBV_\perp}{m_0} \tag{6}$$

$$\frac{\mathrm{d}V_\perp}{\mathrm{dt}} + V_\parallel \frac{\partial V_\perp}{\partial z} = -\frac{\mathrm{eE}}{m_0} + \frac{ev_\parallel B}{m_0} \tag{7}$$

let us define a new variable 'ξ' which depends on space and time as $\xi = z - v_g t$

So $\frac{\partial}{\partial z} \equiv \frac{\partial}{\partial \xi}$ and $\frac{\partial}{\partial t} \equiv -v_g \frac{\partial}{\partial \xi}$

Here $v_g = c\sqrt{\left(1 - \frac{\omega_p{}^2}{\omega^2}\right)}$ is group velocity & $\omega_P = \sqrt{\frac{ne^2}{m\varepsilon_0}}$ is plasma frequency.

From continuity equation $\frac{\partial n}{\partial t} + \vec{\nabla}.\left(n\vec{V}\right) = 0$ (8)

here, n is plasma electron density.

If $n_e{}^I$ represents density perturbation caused by laser pulse propagation, then solving and rewriting Eqs. (6) to (8) yields

$$-v_g \frac{\partial V_\perp}{\partial \xi} + V_\parallel \frac{\partial V_\perp}{\partial \xi} = -\frac{eE}{m_0} + \frac{ev_\parallel B}{m_0} \tag{9}$$

$$-v_g \frac{\partial V_\parallel}{\partial \xi} + V_\parallel \frac{\partial V_\parallel}{\partial \xi} = \frac{e}{m_0}\frac{\partial \phi}{\partial \xi} - \frac{eV_\perp B}{m_0} \tag{10}$$

$$-v_g \frac{\partial n_e{}^I}{\partial \xi} + n_0 \frac{\partial V_\parallel}{\partial \xi} + V_\parallel \frac{\partial n_e{}^I}{\partial \xi} + n_e{}^I \frac{\partial V_\parallel}{\partial \xi} = 0 \tag{11}$$

By solving Eq. (9) to (11) under quasi-static approximation, we obtain general second-order differential equation for generated laser wake potential (Φ) as

$$\left(\frac{\partial^2 \Phi}{\partial \xi^2}\right) + k_P{}^2 \Phi = \left\{\frac{e\left(\beta^2 - 1\right)}{2m_0 v_g{}^2}\right\} E^2 \tag{12}$$

Generated laser wakefield is related to wake potential as

$$E_w = -\frac{d\Phi}{d\xi} \tag{13}$$

The electric field (E) of a plain polarized Hermite–Gaussian laser pulse propagating through homogeneous underdense plasma along z-axis is given by

$$E = \hat{x} E_0 e^{-\frac{(\xi - \frac{L}{2})^2}{r_0^2}} H_s\left(\frac{\sqrt{2}\left(\xi - \frac{L}{2}\right)}{r_0}\right) 0 \le \xi \le L \tag{14}$$

here, E_0 is amplitude of laser electric field, r_0 is laser beam waist, L is the laser pulse length, and s is mode index of Hermite polynomial. The value of Hermite polynomial depends on mode index (s).

Consider a new parameter $\eta = k_p\left(\xi - \frac{L}{2}\right)$. In terms of η, the electron energy gain [36] is accomplished by using the relation

$$\Delta W = \frac{-e}{k_p\left\{1 - \frac{1}{\beta}\right\}} \int_{-k_p L/2}^{\eta} E_w d\eta \tag{15}$$

Equation (12), (13) and (15) can be applied on this laser pulse profile E, to obtain generated laser wake potential (Φ), laser wakefield (E_w) and energy gain by electron (Δ W).

For Hermite mode index s = 0

As per the definition of Hermite polynomial, for s = 0, $H_0\left(\frac{\sqrt{2}\left(\xi - \frac{L}{2}\right)}{r_0}\right) = 1$. So, the solution of Eq. (12), (13) and (15), respectively, is

$$\Phi_0 = -\frac{1}{2}\left\{\frac{e\left(\beta^2 - 1\right)E_0{}^2}{2mv_g{}^2 k_P}\right\} e^{-\frac{1}{8}k_P^2 r_0^2} \sqrt{\frac{\pi}{2}} \left(\mathrm{Erf}\left[\frac{2L - ik_P r_0^2}{2\sqrt{2}r_0}\right] + \mathrm{Erf}\left[\frac{2L + ik_P r_0^2}{2\sqrt{2}r_0}\right]\right) \mathrm{Sin}\left[\frac{1}{2}(L - 2\xi)k_P\right] r_0 \tag{16}$$

$$\mathrm{E}_{w0} = -\frac{1}{2}\left\{\frac{e\left(\beta^2 - 1\right)E_0{}^2}{2mv_g{}^2 k_P}\right\} k_P r_0 e^{-\frac{1}{8}k_P^2 r_0^2} \sqrt{\frac{\pi}{2}} \mathrm{Cos}\left[\frac{1}{2}(L - 2\xi)k_P\right] \left\{\mathrm{Erf}\left[\frac{2L - ik_P r_0^2}{2\sqrt{2}r_0}\right] + \mathrm{Erf}\left[\frac{2L + ik_P r_0^2}{2\sqrt{2}r_0}\right]\right\} \tag{17}$$

$$\Delta \mathrm{W}_0 = \frac{1}{2}\sqrt{\frac{\pi}{2}}\left[\frac{e e^{-\frac{1}{8}k_P^2 r_0^2}(-1 + \beta^2)\mathrm{Cos}\left[\frac{1}{2}(L - \xi)k_P\right]\left(\mathrm{Erf}\left[\frac{2L - ik_P r_0^2}{2\sqrt{2}r_0}\right] + \mathrm{Erf}\left[\frac{2L + ik_P r_0^2}{2\sqrt{2}r_0}\right]\right)\mathrm{Sin}\left[\frac{\xi k_P}{2}\right]E_0^2 r_0}{(1 - \frac{1}{\beta})k_P m_0 v_g^2}\right] \tag{18}$$

Error function (Erf) and imaginary error function (Erfi) are defined [37] as.

Erf [Y] = $\frac{2}{\sqrt{\pi}}\int_0^Y e^{-q^2} dq$ and Erfi [Y] = $\frac{2}{\sqrt{\pi}}\int_0^Y e^{q^2} dq$, respectively.

For Hermite mode index s = 1

For s = 1, $H_1\left(\frac{\sqrt{2}\left(\xi - \frac{L}{2}\right)}{r_0}\right) = 2\left(\frac{\sqrt{2}\left(\xi - \frac{L}{2}\right)}{r_0}\right)$. So, the solution of Eq. (12), (13) and (15), respectively, is

$$\Phi_1 = \frac{1}{16}\left\{\frac{e\left(\beta^2-1\right){E_0}^2}{2m{v_g}^2k_P}\right\}e^{\frac{1}{8}\left(-4i(L+2\xi)k_P-\frac{4L^2}{r_0^2}-k_P^2r_0^2\right)}\left(e^{iLk_P}-e^{2i\xi k_P}\right)$$
$$r_0^2\Bigg\{-8ie^{\frac{1}{8}k_P\left(-4iL+k_Pr_0^2\right)}\left(1+e^{iLk_P}\right)L-4e^{\frac{L^2}{2r_0^2}}\sqrt{2\pi}$$
$$\left(Erf\left(\frac{-2iL+k_Pr_0^2}{2\sqrt{2}r_0}\right)-Erf\left(\frac{2iL+k_Pr_0^2}{2\sqrt{2}r_0}\right)r_0\right)$$
$$+4e^{\frac{1}{8}k_P\left(-4iL+k_Pr_0^2\right)}\left(-1+e^{iLk_P}\right)k_Pr_0^2+e^{\frac{L^2}{2r_0^2}}\sqrt{2\pi}$$
$$\left(Erfi\left(\frac{-2iL+k_Pr_0^2}{2\sqrt{2}r_0}\right)-Erfi\left(\frac{2iL+k_Pr_0^2}{2\sqrt{2}r_0}\right)k_P^2r_0^3\right)\Bigg\} \tag{19}$$

$$\mathrm{E}_{w1} = \frac{1}{8}\left\{\frac{e\left(\beta^2-1\right){E_0}^2}{2m{v_g}^2k_P}\right\}ie^{2i\xi k_P+\frac{1}{8}(-4i(L+2\xi)k_P-\frac{4L^2}{r_0^2}-k_P^2r_0^2)}$$
$$k_P(-8ie^{\frac{1}{8}k_P(-4iL+k_Pr_0^2)}(1+e^{iLk_P})L-4e^{\frac{L^2}{2r_0^2}}\sqrt{2\pi}(\mathrm{Erfi}[\frac{-2iL+k_Pr_0^2}{2\sqrt{2}r_0}]$$
$$-\mathrm{Erfi}[\frac{2iL+k_Pr_0^2}{2\sqrt{2}r_0}])r_0+4e^{\frac{1}{8}k_P(-4iL+k_Pr_0^2)}(-1+e^{iLk_P})k_Pr_0^2$$
$$+e^{\frac{L^2}{2r_0^2}}\sqrt{2\pi}(\mathrm{Erfi}[\frac{-2iL+k_Pr_0^2}{2\sqrt{2}r_0}]-\mathrm{Erfi}[\frac{2iL+k_Pr_0^2}{2\sqrt{2}r_0}])k_P^2r_0^3)$$
$$+\frac{1}{16}ie^{\frac{1}{8}(-4i(L+2\xi)k_P-\frac{4L^2}{r_0^2}-k_P^2r_0^2)}(e^{iLk_P}-e^{2i\xi k_P})k_P(-8ie^{\frac{1}{8}k_P(-4iL+k_Pr_0^2)}$$
$$(1+e^{iLk_P})L-4e^{\frac{L^2}{2r_0^2}}\sqrt{2\pi}(\mathrm{Erfi}[\frac{-2iL+k_Pr_0^2}{2\sqrt{2}r_0}]-\mathrm{Erfi}[\frac{2iL+k_Pr_0^2}{2\sqrt{2}r_0}])r_0$$
$$+4e^{\frac{1}{8}k_P(-4iL+k_Pr_0^2)}(-1+e^{iLk_P})k_Pr_0^2+e^{\frac{L^2}{2r_0^2}}\sqrt{2\pi}(\mathrm{Erfi}[\frac{-2iL+k_Pr_0^2}{2\sqrt{2}r_0}]$$
$$-\mathrm{Erfi}[\frac{2iL+k_Pr_0^2}{2\sqrt{2}r_0}])k_P^2r_0^3) \tag{20}$$

$$\Delta\mathrm{W}_1 = -\frac{1}{32}[\frac{1}{(1-\frac{1}{\beta})k_Pm_0v_g^2}ee^{\frac{1}{8}(-4i(L+2\xi)k_P-\frac{4L^2}{r_0^2}-k_P^2r_0^2)}$$
$$(-1+e^{i\xi k_P})(e^{iLk_P}+e^{i\xi k_P})(-1+\beta^2)E_0^2(-8ie^{\frac{1}{8}k_P(-4iL+k_Pr_0^2)}$$
$$(1+e^{iLk_P})L-4e^{\frac{L^2}{2r_0^2}}\sqrt{2\pi}(\mathrm{Erfi}[\frac{-2iL+k_Pr_0^2}{2\sqrt{2}r_0}]-\mathrm{Erfi}[\frac{2iL+k_Pr_0^2}{2\sqrt{2}r_0}])r_0$$
$$+4e^{\frac{1}{8}k_P(-4iL+k_Pr_0^2)}(-1+e^{iLk_P})k_Pr_0^2+e^{\frac{L^2}{2r_0^2}}\sqrt{2\pi}(\mathrm{Erfi}[\frac{-2iL+k_Pr_0^2}{2\sqrt{2}r_0}]$$
$$-\mathrm{Erfi}[\frac{2iL+k_Pr_0^2}{2\sqrt{2}r_0}])k_P^2r_0^3)] \tag{21}$$

For Hermite mode index s = 2

For s = 2, $H_2\left(\frac{\sqrt{2}\left(\xi-\frac{L}{2}\right)}{r_0}\right) = 4\left(\frac{\sqrt{2}\left(\xi-\frac{L}{2}\right)}{r_0}\right)^2 - 2$. So, the solution of Eq. (12), (13) and (15), respectively, is

$$\Phi_2 = \left\{\frac{e\left(\beta^2-1\right){E_0}^2}{2m{v_g}^2k_P}\right\}\frac{1}{32r_0^2}e^{-i(L+\xi)k_P-\frac{L^2}{2r_0^2}-\frac{1}{8}k_P^2r_0^2}$$
$$(e^{iLk_P}-e^{2i\xi k_P})(-32ie^{\frac{1}{8}k_P^2r_0^2}(1+e^{iLk_P})L^3$$
$$+16e^{\frac{1}{8}k_P^2r_0^2}L(-2i(1+e^{iLk_P})+(-1+e^{iLk_P})Lk_P)$$
$$r_0^2-32e^{\frac{1}{2}L(ik_P+\frac{L}{r_0^2})}\sqrt{2\pi}(\mathrm{Erfi}[\frac{-2iL+k_Pr_0^2}{2\sqrt{2}r_0}]$$
$$-\mathrm{Erfi}[\frac{2iL+k_Pr_0^2}{2\sqrt{2}r_0}])r_0^3+8e^{\frac{1}{8}k_P^2r_0^2}k_P(6(-1+e^{iLk_P})$$
$$+i(1+e^{iLk_P})Lk_P)r_0^4+16e^{\frac{1}{2}L(ik_P+\frac{L}{r_0^2})}\sqrt{2\pi}(\mathrm{Erfi}[\frac{-2iL+k_Pr_0^2}{2\sqrt{2}r_0}]$$
$$-\mathrm{Erfi}[\frac{2iL+k_Pr_0^2}{2\sqrt{2}r_0}])k_P^2r_0^5-4e^{\frac{1}{8}k_P^2r_0^2}(-1+e^{iLk_P})k_P^3r_0^6$$
$$-e^{\frac{1}{2}L(ik_P+\frac{L}{r_0^2})}\sqrt{2\pi}(\mathrm{Erfi}[\frac{-2iL+k_Pr_0^2}{2\sqrt{2}r_0}]$$
$$-\mathrm{Erfi}[\frac{2iL+k_Pr_0^2}{2\sqrt{2}r_0}])k_P^4r_0^7) \tag{22}$$

$$\mathrm{E}_{w2} = \left\{\frac{e\left(\beta^2-1\right){E_0}^2}{2m{v_g}^2k_P}\right\}\frac{1}{16r_0^2}ie^{2i\xi k_P-i(L+\xi)k_P-\frac{L^2}{2r_0^2}-\frac{1}{8}k_P^2r_0^2}$$
$$k_P(-32ie^{\frac{1}{8}k_P^2r_0^2}(1+e^{iLk_P})L^3+16e^{\frac{1}{8}k_P^2r_0^2}L(-2i(1+e^{iLk_P})$$
$$+(-1+e^{iLk_P})Lk_P)r_0^2-32e^{\frac{1}{2}L(ik_P+\frac{L}{r_0^2})}\sqrt{2\pi}$$
$$(\mathrm{Erfi}[\frac{-2iL+k_Pr_0^2}{2\sqrt{2}r_0}]-\mathrm{Erfi}[\frac{2iL+k_Pr_0^2}{2\sqrt{2}r_0}])r_0^3$$
$$+8e^{\frac{1}{8}k_P^2r_0^2}k_P(6(-1+e^{iLk_P})+i(1+e^{iLk_P})Lk_P)r_0^4+16e^{\frac{1}{2}L(ik_P+\frac{L}{r_0^2})}\sqrt{2\pi}$$
$$(\mathrm{Erfi}[\frac{-2iL+k_Pr_0^2}{2\sqrt{2}r_0}]-\mathrm{Erfi}[\frac{2iL+k_Pr_0^2}{2\sqrt{2}r_0}])k_P^2r_0^5$$
$$-4e^{\frac{1}{8}k_P^2r_0^2}(-1+e^{iLk_P})k_P^3r_0^6-e^{\frac{1}{2}L(ik_P+\frac{L}{r_0^2})}\sqrt{2\pi}(\mathrm{Erfi}[\frac{-2iL+k_Pr_0^2}{2\sqrt{2}r_0}]$$
$$-\mathrm{Erfi}[\frac{2iL+k_Pr_0^2}{2\sqrt{2}r_0}])k_P^4r_0^7)+\frac{1}{32r_0^2}ie^{-i(L+\xi)k_P-\frac{L^2}{2r_0^2}-\frac{1}{8}k_P^2r_0^2}$$
$$(e^{iLk_P}-e^{2i\xi k_P})k_P(-32ie^{\frac{1}{8}k_P^2r_0^2}(1+e^{iLk_P})L^3+16e^{\frac{1}{8}k_P^2r_0^2}L(-2i(1+e^{iLk_P})$$
$$+(-1+e^{iLk_P})Lk_P)r_0^2-32e^{\frac{1}{2}L(ik_P+\frac{L}{r_0^2})}\sqrt{2\pi}(\mathrm{Erfi}[\frac{-2iL+k_Pr_0^2}{2\sqrt{2}r_0}]$$
$$-\mathrm{Erfi}[\frac{2iL+k_Pr_0^2}{2\sqrt{2}r_0}])r_0^3+8e^{\frac{1}{8}k_P^2r_0^2}k_P(6(-1+e^{iLk_P})+i(1+e^{iLk_P})Lk_P)r_0^4$$
$$+16e^{\frac{1}{2}L(ik_P+\frac{L}{r_0^2})}\sqrt{2\pi}(\mathrm{Erfi}[\frac{-2iL+k_Pr_0^2}{2\sqrt{2}r_0}]$$
$$-\mathrm{Erfi}[\frac{2iL+k_Pr_0^2}{2\sqrt{2}r_0}])k_P^2r_0^5-4e^{\frac{1}{8}k_P^2r_0^2}(-1+e^{iLk_P})k_P^3r_0^6-e^{\frac{1}{2}L(ik_P+\frac{L}{r_0^2})}$$
$$\sqrt{2\pi}(\mathrm{Erfi}[\frac{-2iL+k_Pr_0^2}{2\sqrt{2}r_0}]-\mathrm{Erfi}[\frac{2iL+k_Pr_0^2}{2\sqrt{2}r_0}])k_P^4r_0^7) \tag{23}$$

$$\Delta W_2 = -\frac{1}{64}[\frac{1}{(1-\frac{1}{\beta})k_P m_0 r_0^2 v_g^2} ee^{-i(L+\xi)k_P - \frac{L^2}{2r_0^2} - \frac{1}{8}k_P^2 r_0^2}$$
$$(-1+e^{i\xi k_P})(e^{iLk_P}+e^{i\xi k_P})(-1+\beta^2)$$
$$E_0^2(-32ie^{\frac{1}{8}k_P^2 r_0^2}(1+e^{iLk_P})L^3 + 16e^{\frac{1}{8}k_P^2 r_0^2}$$
$$L(-2i(1+e^{iLk_P}) + (-1+e^{iLk_P})Lk_P)r_0^2$$
$$- 32e^{\frac{1}{2}L(ik_P+\frac{L}{r_0^2})}\sqrt{2\pi}(\text{Erfi}[\frac{-2iL+k_P r_0^2}{2\sqrt{2}r_0}]$$
$$- \text{Erfi}[\frac{2iL+k_P r_0^2}{2\sqrt{2}r_0}])r_0^3 + 8e^{\frac{1}{8}k_P^2 r_0^2}k_P(6(-1+e^{iLk_P})$$
$$+ i(1+e^{iLk_P})Lk_P)r_0^4 + 16e^{\frac{1}{2}L(ik_P+\frac{L}{r_0^2})}$$
$$\sqrt{2\pi}(\text{Erfi}[\frac{-2iL+k_P r_0^2}{2\sqrt{2}r_0}] - \text{Erfi}[\frac{2iL+k_P r_0^2}{2\sqrt{2}r_0}])k_P^2 r_0^5$$
$$- 4e^{\frac{1}{8}k_P^2 r_0^2}(-1+e^{iLk_P})k_P^3 r_0^6 - e^{\frac{1}{2}L(ik_P+\frac{L}{r_0^2})}$$
$$\sqrt{2\pi}(\text{Erfi}[\frac{-2iL+k_P r_0^2}{2\sqrt{2}r_0}] - \text{Erfi}[\frac{2iL+k_P r_0^2}{2\sqrt{2}r_0}])k_P^4 r_0^7)] \quad (24)$$

Equations (16) to(24) are the outcomes of LWFA effect for various Hermite–Gaussian pulse profiles, which depend on various factors like beam waist (r_0), pulse length (L), propagation distance (ξ), mode index (s), plasma propagation constant (k_P), laser field amplitude (E_0), etc.

Results and discussion

In this paper, we have chosen plasma of electron density $2\times10^{23}m^{-3}$, plasma frequency $2.52\times10^{13}rad/s$. Laser pulse of wavelength $10.6\mu m$, laser frequency $1.78\times10^{14}rad/s$, and pulse length $48.10\mu m$ are chosen for numerical investigation. Amplitude of laser electric field (E_0) is chosen as $2.15\times10^{11}V/m$, $4.30\times10^{11}V/m$ and $8.60\times10^{11}V/m$ to investigate LWFA effect.

Figure 1 shows the variation of energy gain by electrons as a function of propagation distance for $E_0 = 4.30\times10^{11}V/m$. Peak of all 3 curves corresponding to Hermite mode indexed values s = 0, s = 1 and s = 2 in the figure lies at the same position ($\xi = 31.45\mu m$). Maximum energy gain is 470.10 MeV for s = 2 mode and minimum energy gain is 39.42 MeV for s = 1 mode. For s = 0, energy gain is 167.65 MeV for the same other parameters. So, it can be concluded that increment of energy gain depends on the mode of Hermite polynomial.

Figure 2 shows the variation of maximum energy gain with beam waist for different laser field amplitudes (E_0). For all Hermite polynomial mode indexes (s = 0, 1, 2), the maximum energy gain by electrons increases with increase in laser field amplitude as E_0^2. For s = 0, energy gain increases rapidly with increase in beam waist up to a value of $25.35\mu m$, then attains its maximum value and becomes constant with further increase in beam waist. A maximum of 696 MeV energy gain is obtained for laser field amplitude $8.60\times10^{11}V/m$. For s = 1, electron energy gain increases rapidly till beam waist $16.90\mu m$, then decreases sharply with further increase in beam waist and becomes almost zero for beam waist greater than $70\mu m$. A maximum of 647.2 MeV energy gain is obtained for beam waist $13.52\mu m$ and laser field amplitude $8.60\times10^{11}V/m$. For s = 2, electron energy gain increases rapidly till beam waist $10.14\mu m$, then decreases till $20.28\mu m$, and finally increases with further increase in bream waist and becomes constant for beam waist greater than $70\mu m$. A maximum energy gain of 2652.54 MeV is obtained with selected parameters in this case. So, the effect of beam waist on energy gained by the electrons depends on the Hermite mode index of chosen pulse profile.

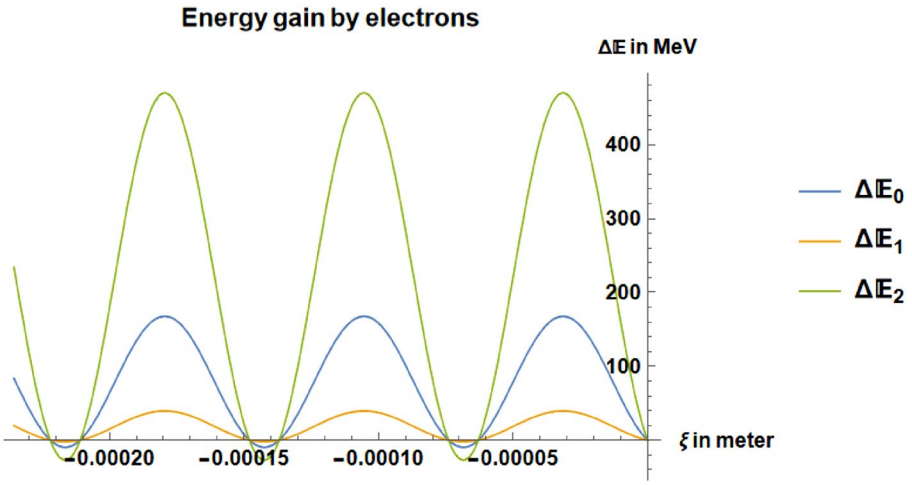

Fig. 1 Variation of energy gain by electron with propagation distance for various Hermite mode indexes, s = 0 (ΔE_0), s = 1 (ΔE_1) and s = 2 (ΔE_2) for $E_0 = 4.30\times10^{11}V/m$, $r_0 = 33.74\mu m$ and $L = 48.10\mu m$. Other parameters are same as defined above

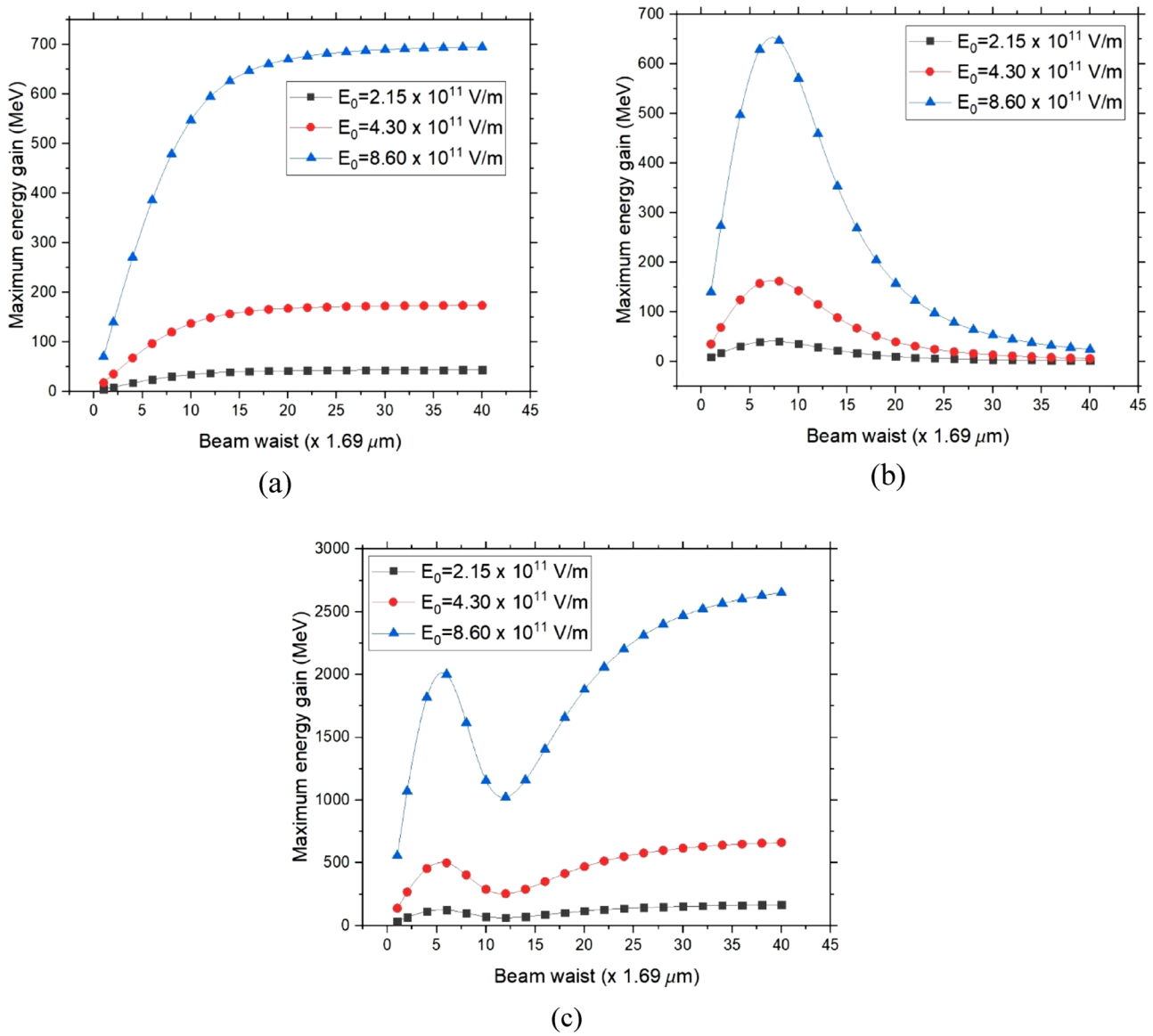

Fig. 2 Variation of energy gain by electron with beam waist for various Hermite mode indexes, s = 0 **a**, s = 1 **b** and s = 2 **c** for $L = 48.10\mu m$ Other parameters are same as defined above

Hermite polynomial term $H_s(x) where x = \left(\frac{\sqrt{2}\left(\xi - \frac{L}{2}\right)}{r_0}\right)$ is a part of the selected laser pulse profile. With the variation in s value, Hermite polynomial and laser pulse profile also vary. Variation in laser pulse profile is responsible for energy enhancement.

Variation of energy gain by electrons with beam waist and laser pulse length is illustrated in Fig. 3. For s = 0 mode, energy gain becomes constant for higher values of beam waist if pulse length is small (< 0.0015 m). If the pulse length is increased further, periodic variation in energy gain with beam waist is obtained for smaller beam waist ($0 < r_0 < 50\mu m$) but energy gain becomes zero for higher values of beam waist. Similar variation can be seen for s = 1 mode, but the maximum energy gain is obtained for $20\mu m < r_0 < 70\mu m$. Similarly, for s = 2 mode, the maximum energy gain is obtained for beam waist range$40\mu m < r_0 < 100\mu m$. So, the range of beam waist corresponding to maximum energy gain depends on Hermite mode index as well as pulse length also and shifts toward higher beam waist with increase in Hermite mode index.

Figure 4 illustrates the variation of energy gain by electrons with plasma density for different Hermite mode indexes. For s = 0 and s = 2 mode, energy gain oscillates with increasing amplitude till the condition of over dense plasma

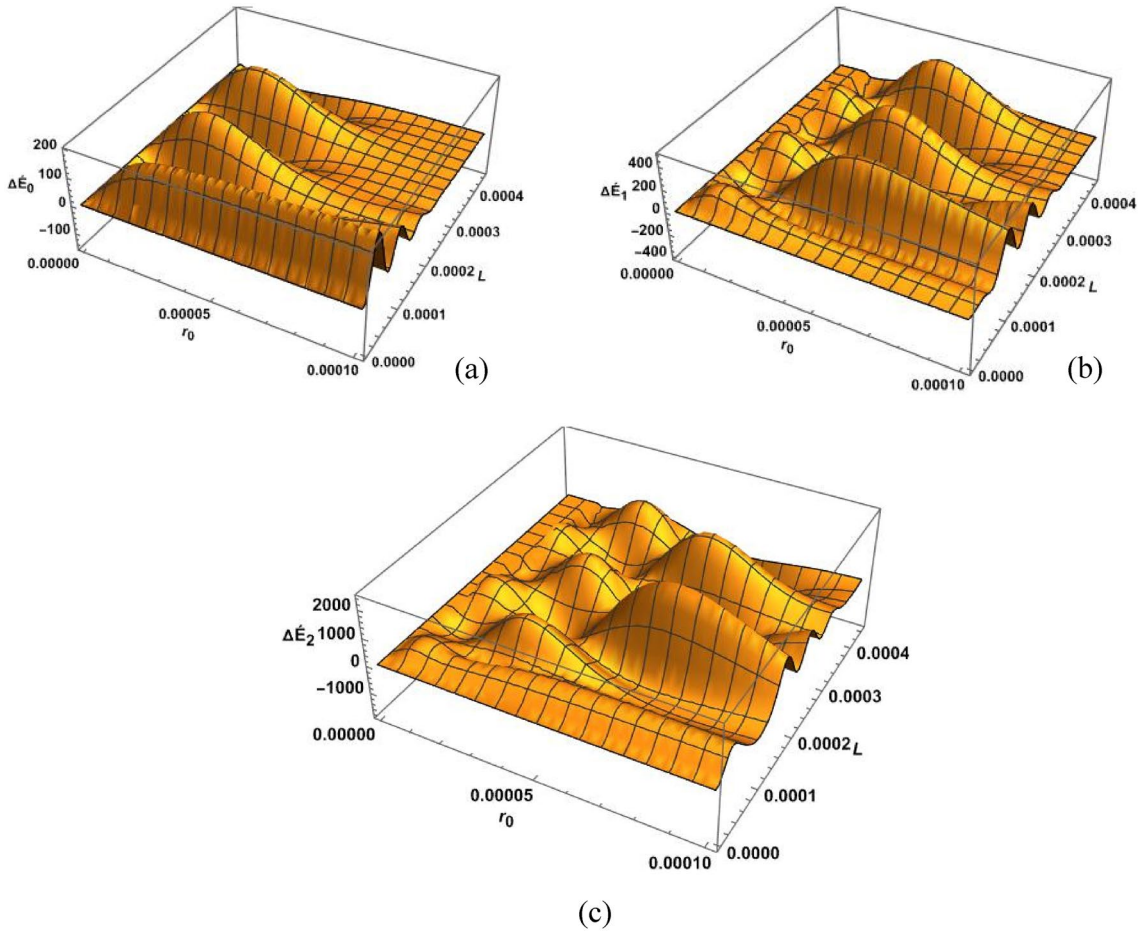

Fig. 3 Variation of energy gain by electron with beam waist and pulse length for various Hermite mode indexes, s = 0 **a**, s = 1 **b** and s = 2 **c** for $E_0 = 4.30 \times 10^{11} V/m$. Other parameters are same as defined above. r_0 and L are in meter and ΔE is in MeV units

$(\omega_p > \omega_L)$ is achieved. But for s = 1 mode, the variation is just the opposite. Amplitude of oscillating energy gain decreases rapidly with increase in plasma density. Energy gain becomes almost zero for the plasma of higher plasma density for s = 1 mode but a maximum energy gain with higher plasma density is obtained for s = 0 and s = 0 mode. It is due to complex structure of Hermite–Gaussian laser pulse.

In this study, we have obtained a maximum energy gain of 2.65 GeV is obtained for $E_0 = 8.60 \times 10^{11} V/m$, $r_0 = 70\mu m, L = 48.10\mu m$ and plasma density $2 \times 10^{23} m^{-3}$.

The outcomes of this study are consistent with the study of Ghotra et al. [38]. In their investigation, they used circular polarized Hermite–Gaussian laser pulse to accelerate electrons by direct laser acceleration (DLA) phenomenon for different Hermite mode indexes. They observed that enhanced electron energy gain can be obtained for even Hermite mode index as compared to odd Hermite mode indexes. In an experimental study done by Oumbarek et al. [39], it is observed that generated laser wakefield acceleration depends on laser profile. A complex laser pulse profile can develop a more effective, energy efficient acceleration scheme as compared to a simple Gaussian laser pulse.

Conclusion

Using Hermite–Gaussian laser pulses, the research studies the phenomena of laser wakefield acceleration in a collisionless underdense plasma. The research investigates the delicate interplay between the laser pulse's properties, the ensuing laser wakefield structure, and the electron energy gain using theoretical analysis. In our study, we observed that the electron energy gain grows as the amplitude of the laser pulse increases, regardless of the Hermite mode index. Under identical conditions, we observed enhanced energy gain for s = 0 and s = 2 mode indexes than for s = 1 mode. For a given Hermite mode index, electron energy gain varies with pulse length, plasma density, and beam waist. As a result, the optimized value of any one parameter for optimum energy gain swings together with the values of the

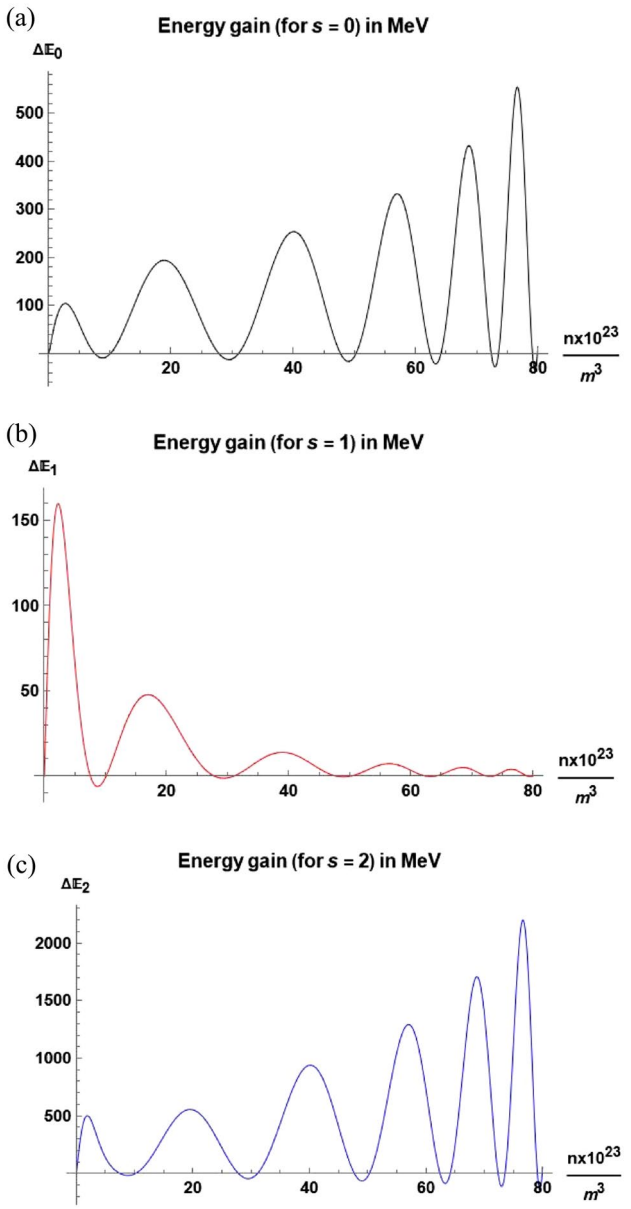

Fig. 4 Variation of energy gain by electron with beam waist and pulse length for various Hermite mode indexes, s = 0 **a**, s = 1 **b** and s = 2 **c** for $E_0 = 4.30 \times 10^{11} V/m, r_0 = 10.12 \mu m and L = 48.10 \mu m$. Other parameters are same as defined above

other two parameters. With a certain combination of conditions, we were able to attain an energy increase of 2.65 GeV. The findings shed light on the ability of Hermite–Gaussian laser pulses to improve the performance of LWFA experimental setups, providing insights into optimizing the generation of high-energy particle beams for a variety of applications, including particle physics experiments and medical treatments.

Author contributions VK contributed to derivation, methodology, analytical modeling and graph plotting; VT contributed to supervision, reviewing, and editing.

Funding Not applicable.

Data availability The data that support the findings of this study are available from the corresponding authors upon reasonable request.

Declarations

Conflict of interest The authors declare no competing interest.

Ethical approval Not applicable.

Consent to participate Not applicable.

Consent for Publication Not applicable.

References

1. A.E. Hussein et al., Laser-wakefield accelerators for high-resolution X-ray imaging of complex microstructures. Sci. Rep. **9**(1), 3249 (2019)
2. M. Asadi Asadabad, M. Jafari Eskandari, Transmission electron microscopy as best technique for characterization in nanotechnology. Synth. React. Inorg. Metal-Org.Nano-Metal Chem. **45**(3), 323–326 (2015)
3. N. Marzari, A. Ferretti, C. Wolverton, Electronic-structure methods for materials design. Nat. Mater. **20**(6), 736–749 (2021)
4. M.G. Ronga et al., Back to the future: very high-energy electrons (VHEEs) and their potential application in radiation therapy. Cancers (Basel) **13**(19), 4942 (2021)
5. E. Amato, S. Casanova, On particle acceleration and transport in plasmas in the Galaxy: theory and observations. J. Plasma Phys. **87**(1), 845870101 (2021)
6. F.W. Low, C.W. Lai, Recent developments of graphene-TiO_2 composite nanomaterials as efficient photoelectrodes in dye-sensitized solar cells: A review. Renew. Sustain. Energy Rev. **82**, 103–125 (2018)
7. A.V. Ponomarev, B.G. Ershov, The green method in water management: electron beam treatment. Environ. Sci. Technol. **54**(9), 5331–5344 (2020)
8. M. Vadrucci, A machine for ionizing radiation treatment of biodeteriogens infesting artistic objects. Quantum Beam Sci **6**(4), 33 (2022)
9. T. Tajima and J. M. Dawson (1979), Laser electron accelerator,
10. S. Kumar, S. Vij, N. Kant, V. Thakur, Resonant terahertz generation by the interaction of laser beams with magnetized anharmonic carbon nanotube array. Plasmonics **17**(1), 381–388 (2022)
11. S. Kumar, S. Vij, N. Kant, V. Thakur, Resonant terahertz generation by cross-focusing of Gaussian laser beams in the array of vertically aligned anharmonic and magnetized CNTs. OptCommun **513**, 128112 (2022)
12. H.K. Midha, V. Sharma, N. Kant, V. Thakur, Efficient THz generation by Hermite-cosh-Gaussian lasers in plasma with slanting density modulation. J. Opt. (2023). https://doi.org/10.1007/s12596-023-01413-5

13. S. Kumar, S. Vij, N. Kant, A. Mehta, V. Thakur, Resonant terahertz generation from laser filaments in the presence of static electric field in a magnetized collisional plasma. European Phys. J. Plus **136**(2), 148 (2021)
14. S. Kumar, S. Vij, N. Kant, V. Thakur, Combined effect of transverse electric and magnetic fields on THz generation by beating of two amplitude-modulated laser beams in the collisional plasma. J. Astrophys. Astron. **43**(1), 30 (2022)
15. S. Kumar, S. Vij, N. Kant, V. Thakur, Interaction of obliquely incident lasers with anharmonic CNTs acting as dipole antenna to generate resonant THz radiation. Waves Random Complex Media (2022). https://doi.org/10.1080/17455030.2022.2155330
16. S. Kumar, N. Kant, V. Thakur, THz generation by self-focused Gaussian laser beam in the array of anharmonic VA-CNTs. Opt Quant. Electron **55**(3), 281 (2023)
17. V. Thakur, N. Kant, Resonant second harmonic generation by a chirped laser pulse in a semiconductor. Optik (Stuttg) **130**, 525–530 (2017)
18. V. Thakur, S. Vij, V. Sharma, N. Kant, Influence of exponential density ramp on second harmonic generation by a short pulse laser in magnetized plasma. Optik (Stuttg) **171**, 523–528 (2018)
19. V. Sharma, V. Thakur, A. Singh, N. Kant, Third harmonic generation of a relativistic self-focusing laser in plasma under exponential density ramp. Zeitschrift fur Naturforschung - Section A Journal of Physical Sciences **77**(4), 323–328 (2022)
20. V. Thakur, N. Kant, Effect of pulse slippage on density transition-based resonant third-harmonic generation of short-pulse laser in plasma. Front Phys. (Beijing) **11**(4), 115202 (2016)
21. V. Thakur, N. Kant, Stronger self-focusing of a chirped pulse laser with exponential density ramp profile in cold quantum magnetoplasma. Optik (Stuttg) **172**, 191–196 (2018)
22. V. Thakur, N. Kant, Stronger self-focusing of cosh-Gaussian laser beam under exponential density ramp in plasma with linear absorption. Optik (Stuttg) **183**, 912–917 (2019)
23. E. Esarey, C.B. Schroeder, W.P. Leemans, Physics of laser-driven plasma-based electron accelerators. Rev. Mod. Phys. **81**(3), 1229–1285 (2009)
24. V. Sharma, S. Kumar, N. Kant, V. Thakur, Excitation of the Laser wakefield by asymmetric chirped laser pulse in under dense plasma. J. Opt. (2023). https://doi.org/10.1007/s12596-023-01326-3
25. H.R. Askari, A. Shahidani, Effect of magnetic field on production of wake field in laser–plasma interactions: Gaussian-like (GL) and rectangular–triangular (RT) pulses. Optik – Int. J. Light Electron Opt. **124**(17), 3154–3161 (2013)
26. R. Fallah, S.M. Khorashadizadeh, Electron acceleration in a homogeneous plasma by Bessel-Gaussian and Gaussian pulses. Contrib. Plasma Phys. **58**(9), 878–889 (2018)
27. V. Sharma, S. Kumar, To study the effect of laser frequency-chirp on trapped electrons in laser wakefield acceleration. J. Phys. Conf. Ser. **2267**(1), 012097 (2022)
28. V. Sharma, S. Kumar, N. Kant, V. Thakur, Effect of frequency chirp and pulse length on laser wakefield excitation in under-dense plasma. Braz. J. Phys. **53**(6), 157 (2023)
29. M. Abedi-Varaki, M.E. Daraei, Impact of wiggler magnetic field on wakefield generation and electron acceleration by Gaussian, super-Gaussian and Bessel-Gaussian laser pulses propagating in collisionless plasma. J. Plasma Phys. **89**(1), 905890114 (2023)
30. V. Sharma, S. Kumar, N. Kant, V. Thakur, Enhanced laser wakefield acceleration by a circularly polarized laser pulse in obliquely magnetized under-dense plasma. Opt Quantum Electron **55**(13), 1150 (2023)
31. H.S. Ghotra, Laser wakefield and direct laser acceleration of electron by chirped laser pulses. Optik (Stuttg) **260**, 169080 (2022)
32. R. Fallah, S.M. Khorashadizadeh, Influence of Gaussian, super-Gaussian, and cosine-Gaussian pulse properties on the electron acceleration in a homogeneous plasma. IEEE Trans. Plasma Sci. **46**(6), 2085–2090 (2018)
33. D.N. Gupta, M. Yadav, A. Jain, S. Kumar, Electron bunch charge enhancement in laser wakefield acceleration using a flattened Gaussian laser pulse. Phys. Lett., Sect. A: General Atomic Solid State Phys. **414**, 127631 (2021)
34. V. Sharma, S. Kumar, N. Kant, V. Thakur, Enhanced laser wakefield by beating of two co-propagating Gaussian laser pulses. J. Opt. (2023). https://doi.org/10.1007/s12596-023-01250-6
35. K. Gopal, D.N. Gupta, H. Suk, Pulse-length effect on laser wakefield acceleration of electrons by skewed laser pulses. IEEE Trans. Plasma Sci. **49**(3), 1152–1158 (2021)
36. M. Abedi-Varaki, N. Kant, Magnetic field-assisted wakefield generation and electron acceleration by Gaussian and super-Gaussian laser pulses in plasma. Mod. Phys. Lett. B **36**, 07 (2022)
37. N.H. Mohammed, N.E. Cho, E.A. Adegani, T. Bulboaca, Geometric properties of normalized imaginary error function. Studia Universitatis Babes-Bolyai Matematica **67**(2), 455–462 (2022)
38. H.S. Ghotra, N. Kant, TEM modes influenced electron acceleration by Hermite–Gaussian laser beam in plasma. Laser Part. Beams **34**(3), 385–393 (2016)
39. D. Oumbarek Espinos et al., Notable improvements on LWFA through precise laser wavefront tuning. Sci Rep **13**(1), 18466–98 (2023)